Jinst

Published by IOP Publishing for Sissa Medialab

Received: *March 14, 2023*
Accepted: *April 28, 2023*
Published: *May 26, 2023*

NUV-HD SiPMs with metal-filled trenches

Stefano Merzi,[a,*] **Stefan E. Brunner,**[b] **Alberto Gola,**[a] **Alessandro Inglese,**[b] **Alberto Mazzi,**[a] **Giovanni Paternoster,**[a] **Michele Penna,**[a] **Claudio Piemonte**[b] **and Maria Ruzzarin**[a]

[a] *Fondazione Bruno Kessler (FBK), Center for Sensors and Devices (SD), Via Sommarive 18, Trento I-38123, Italy*
[b] *Broadcom Inc., 2 Wernerwerkstrasse, Regensburg 93049, Germany*

E-mail: smerzi@fbk.eu

Abstract: In this paper we present the performance of a new SiPM that is sensitive to blue light and features narrow metal-filled trenches placed in the area around the single-photon avalanche diodes (SPADs) that allow an almost complete suppression the internal optical crosstalk. In particular, we show the benefits of this technological upgrade in terms of electro-optical SiPM performance when compared to the previous technology which had only a partial optical screening between the SPADs. The most relevant effect is the much higher bias voltage that can be applied to the new device before the noise diverges. This allows to optimize and improve both the photon-detection efficiency and the single-photon time resolution. We also coupled the SiPMs to LYSO scintillators to verify the performance for possible application in Positron-Emission Tomography. Thanks to the better electro-optical features we were able to measure an improved coincidence time resolution. Furthermore, the optimal voltage operation region is substantially larger, making this SiPM more suitable for real system application where thousands of channels have to provide stable and reproducible performance.

Keywords: Detector design and construction technologies and materials; Photon detectors for UV, visible and IR photons (solid-state) (PIN diodes, APDs, Si-PMTs, G-APDs, CCDs, EBCCDs, EMCCDs, CMOS imagers, etc); Solid state detectors; Gamma camera, SPECT, PET PET/CT, coronary CT angiography (CTA)

*Corresponding author.

https://doi.org/10.1088/1748-0221/18/05/P05040

2023 JINST 18 P05040

Contents

1 Introduction

In recent years, continuous improvements in the performance of Silicon Photomultipliers (SiPMs) increased their attractiveness for several applications that require high detection speed, high sensitivity and low noise, such as Positron Emission Tomography (PET) and Time-of-Flight PET (ToF-PET) medical apparatus [1], automotive Lidar [2] and physics experiments [3]. Each application has its own specific requirements in terms of wavelength sensitivity, timing resolution, and dynamic range. In this paper we focus on the medical imaging applications, which mostly employ near ultraviolet sensitive SiPMs (NUV-SiPM) thanks to the excellent overlap between their Photon Detection Efficiency (PDE) spectrum and the emission spectrum of conventional inorganic scintillators such as LSO or LYSO. Moreover, NUV-sensitive SiPMs from several manufacturers offer a low noise level and fast timing performance with a coincidence time resolution of a few hundreds of picoseconds in commercially available apparatus [4].

The development of next generation ToF-PET systems envisions a further reduction of the Coincidence Time Resolution (CTR) to improve the signal-to-noise ratio and spatial resolution of the tomographic image for a given number of detected coincidences and, in turn, benefits the patients, thanks to a reduction of the radiation dose and time needed for the measurement. In the context of SiPMs, CTR can be improved by increasing the PDE and/or by reducing the Single Photon Time Resolution (SPTR) [1]. Both PDE and SPTR improve with the excess bias (i.e. the difference between the bias voltage and the breakdown voltage) until they reach a saturation thus, theoretically, also the CTR could be improved by increasing the excess bias of the SiPM. However, the limit to this approach is the increase of the correlated noise of the detector with the excess bias, which deteriorates the CTR before the detector reaches the saturation of PDE and SPTR [5]–[7]. For this reason, suppression of correlated noise and in particular optical crosstalk, becomes a focal point for the development of next-generation ToF-PET detectors. In this regard, a relevant improvement came to the field with the development of optically insulating trenches (also called DTI, Deep Trench Isolation) between microcells in a SiPM, first introduced in a commercial product by Hamamatsu MPPC-LCT4 detectors [8].

2023 JINST 18 P05040

Recently, within a collaboration between Broadcom and Fondazione Bruno Kessler (FBK), the FBK NUV-HD SiPM technology has been upgraded with metal-filled deep trench isolation (NUV-HD-MT or, in case of Broadcom products, simply NUV-MT). The metal layer acts as a reflector for the photons emitted during the avalanche (secondary photons), confining them within the same fired microcell and suppressing the internal crosstalk probability.

In this paper we will show the results of the electro-optical characterization of this upgraded technology highlighting the benefits of the crosstalk suppression, compared to the NUV-HD technology, in terms of extended dynamic range that allows to reliably operate these detectors at very high excess bias, thus reaching high values of PDE and Gain that translates into an improved CTR performance.

2 Detector structure and design

The starting point of the new SiPM development is the NUV-HD technology [9]. It features DTIs between the SPADs (Single-Photon Avalanche Diodes) which are filled with silicon oxide. This material provides an excellent electrical insulation whereas the change in index of refraction provides a partial optical insulation, thus bringing a significant improvement compared to the previous NUV technology [10]. However its transparency still allows part of the photons to travel from one SPAD to the other. The insertion of an opaque/reflective metal layer inside the deep trench isolation allows a complete suppression of the photon transmission between cells and thus the internal optical crosstalk of the device. This article reports studies conducted on devices that are the results of an optimization process of the total width of the trench, which was carried out on several propaedeutic experiments that aimed at simultaneously maintaining high electrical and optical isolation between neighboring microcells. Furthermore, in the same experiments, we tested different distances of the high-field region from the trench. This is important to avoid premature breakdown at the edge of the active area. As a result of this study, we found an optimal edge/trench design which allowed us to reach very high Fill Factor (FF), only 2% lower compared to the same cell sizes of the standard NUV-HD technology (see table 1).

Table 1. Fill Factor as a function of the microcell size for the two different technologies, the standard NUV-HD and the new NUV-HD-MT with metal-filled trenches.

Cell size	NUV-HD FF	NUV-HD-MT FF
40 µm	82.8%	81.1%
45 µm	84.7%	83.3%
50 µm	86.3%	85.0%

As shown in the table, we produced SiPMs with three different cell sizes of 40, 45 and 50 µm, respectively, whereas, in terms of device size, we produced SiPMs with about $4 \times 4\,\mathrm{mm}^2$ for each variant of cell size and $1 \times 1\,\mathrm{mm}^2$ for the 40 and 45 µm cell size variant. Measuring and comparing these design variants, we could evaluate the behavior of the new technology for the TOF-PET application.

In addition to the change in the trench technology described above we also modified the layout of the top metal lines compared to what we used in the FBK NUV-HD technology, as shown in

2023 JINST 18 P05040

figure 1. Previous design of the metal lines used a "comb-like" structure. In the new NUV-HD-MT devices we designed a "grid-like" metal structure, with horizontal and vertical lines connecting all SPADs to the bonding pads. This design allows for a reduction of the parasitic resistance of the metal connection especially for the SPADs placed far away from the bonding pad.

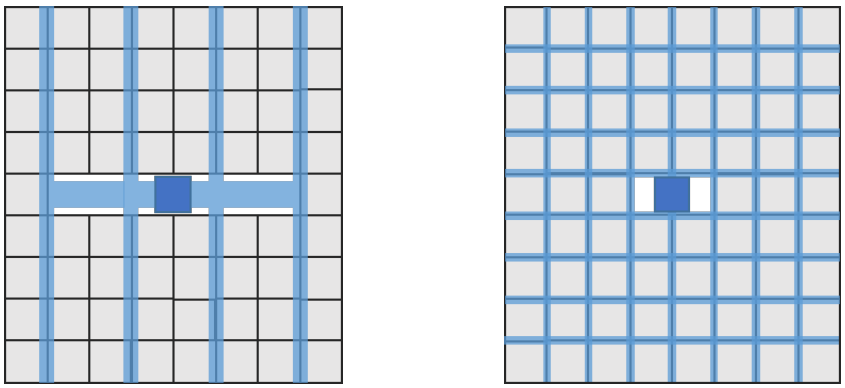

(a) (b)

Figure 1. Schematic representation of the metal lines layout in the "comb-like" structure (a) and "grid-like" structure (b). The SPADs are the light gray squares with the metal-filled DTIs in black. The metal lines are represented in light blue, superimposed on the DTIs, and the central bonding as a dark blue square.

3 Detector characterization

In this section we present the results of the characterization of this NUV-HD-MT technology and compare it with its predecessor, i.e. NUV-HD. The tests are carried out in three steps. The first one is current-voltage measurement in dark conditions, and at different temperatures. The second is the electro-optical characterization on the packaged device and the third is the application-related evaluation of the device coupled with scintillators.

3.1 Analysis of current-voltage characteristics

Figure 2 shows an example of the measured current-voltage (IV) curves (normalized for the detector area) for a NUV-HD-MT $4 \times 4\,\mathrm{mm}^2$ SiPM with 40 µm microcell size compared to a NUV-HD $3 \times 3\,\mathrm{mm}^2$ SiPM with 40 µm microcell. The new device shows a breakdown voltage of 32.2 V, similar to the previous version. On the other hand, the operating range is greatly extended having the current divergence at around 55 V instead of 43 V. This translates into a max excess bias of about 23 V (figure 2(b)). As it will be shown later, while the current divergence of the NUV-HD SiPMs is caused by the diverging crosstalk probability, for the NUV-HD-MT SiPM, it is likely due to either bad-quenching of the avalanche discharge (reached when the current flowing through the device does not allow a fluctuation to zero of the number of carriers drifting through the junction) [11]–[13] or to edge breakdown (reached when the electric field at the periphery of the junction is high enough to create a second avalanche region).

Current-voltage characteristics were also taken at different temperatures in the range −60°C to +70°C in 5°C steps. Results are shown in figure 3(a) in which, for better clarity, only some of

2023 JINST 18 P05040

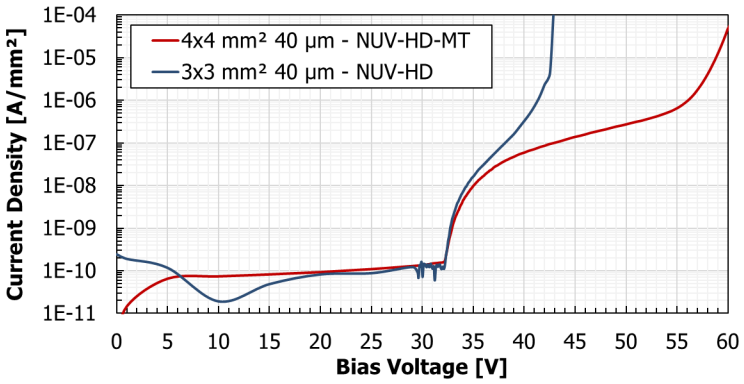

(a)

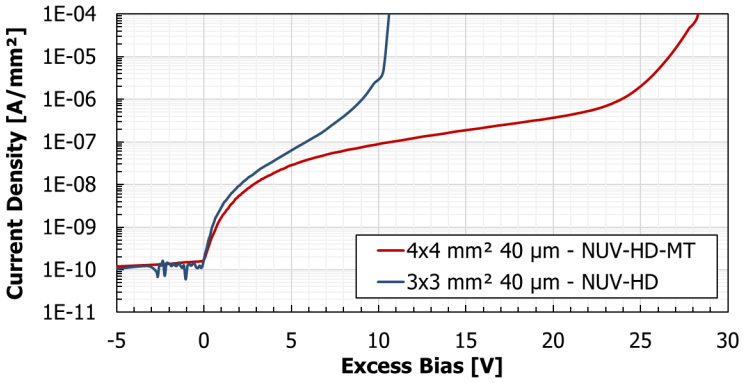

(b)

Figure 2. IV curve of a $4 \times 4\,\mathrm{mm}^2$ NUV-HD-MT SiPM and a $3 \times 3\,\mathrm{mm}^2$ NUV-HD SiPM with 40 µm cell size. (a): current density as a function of the bias voltage. (b): current density as function the excess bias.

the curves are shown, including the calculation of breakdown voltage at each temperature. The resulting breakdown voltage temperature coefficient is extracted from the fit of the points above −25°C, in figure 3(b). For lower temperatures the calculation of the breakdown is less precise due to the noise introduced by the measurement setup at very low currents. The resulting breakdown voltage temperature coefficient is 31 mV/°C, in agreement with what was measured for the previous FBK NUV-HD technology [9].

The dark current at a given excess bias voltage can be also evaluated to understand the dominant mechanism of carrier generation. Figure 3(c) shows the Arrhenius plot of the current at 5 V of excess bias as a function of 1000/T. The activation energy was calculated by fitting the most linear region, i.e., around room temperature, in the range −20°C to +20°C (or $3.41\,\mathrm{K}^{-1}$ to $3.95\,\mathrm{K}^{-1}$ in 1000/T units). Repeating this fit at different excess biases, the activation energy as a function of the excess bias was calculated, as shown in figure 3(d). The plot shows an activation energy between 0.6 and 0.5 eV, which is around mid-bandgap for the silicon, decreasing with excess bias due to the effect of the high electric field in the microcells.

3.2 Functional characterization in dark conditions

Functional characterization of the SiPMs in dark conditions was performed in a thermostatic chamber at a controlled temperature of 20°C, following the method described in [14]. The first

2023 JINST 18 P05040

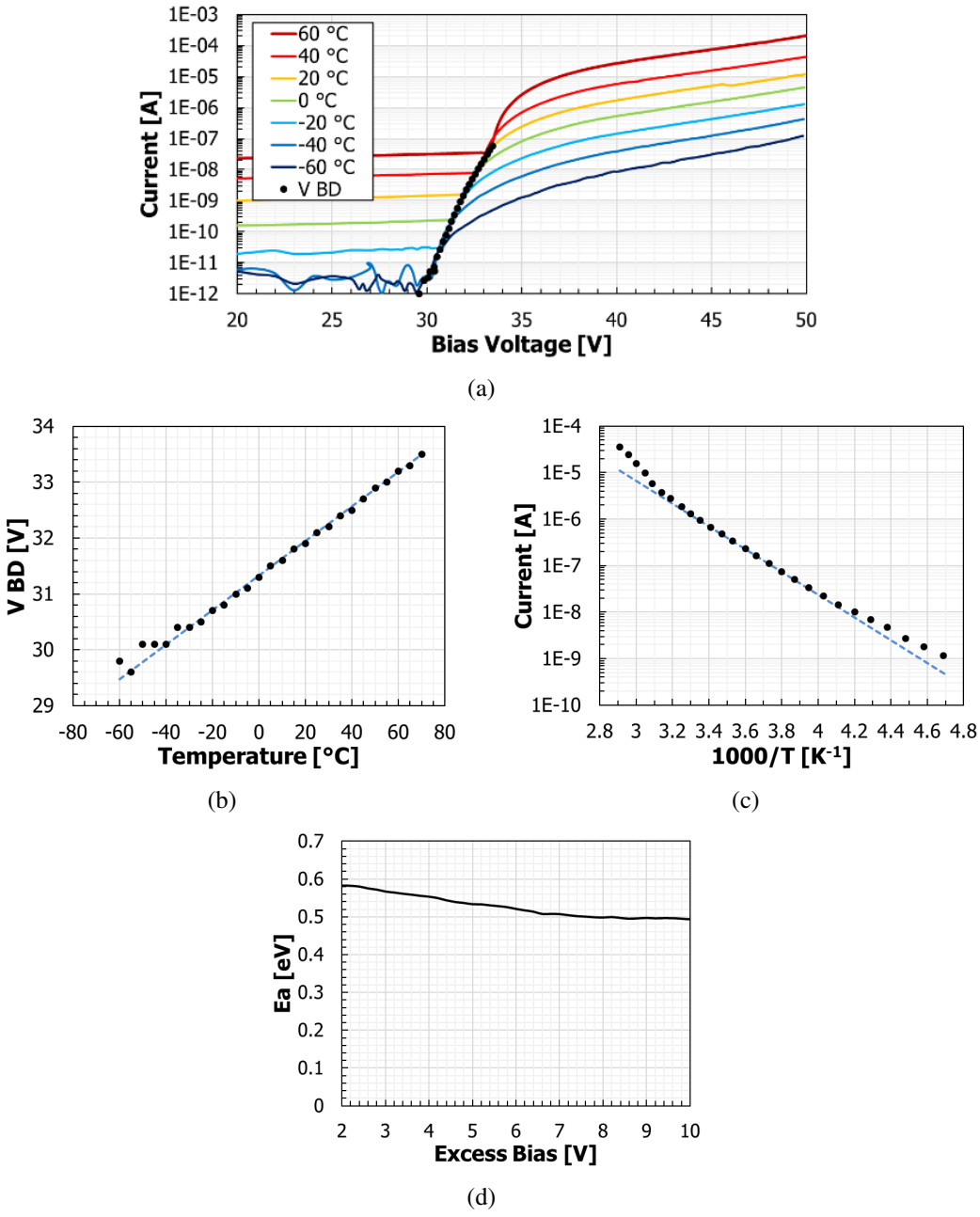

Figure 3. (a): IV curves of a $4 \times 4\,\mathrm{mm}^2$ NUV-HD-MT SiPM with 45 µm cell size taken at different temperatures and calculated breakdown voltages (dots). (b): breakdown voltage as a function of the temperature. (c): current measured at 5 V of excess bias as a function of 1000/T. The dashed lines represent the fit for the calculation of the activation energy, calculated in the most linear part, between −20°C and +20°C. (d): activation energy as a function of the excess bias.

round of tests was done on $1 \times 1\,\mathrm{mm}^2$ SiPM chips mounted on a PCB socket without encapsulation. In figure 4 the main parameters extracted in the study are reported. In particular, we compare the results of the three different SPAD sizes (40, 45 and 50 µm) of NUV-HD-MT SiPM and the standard NUV-HD SiPM with 40 µm cell size.

2023 JINST 18 P05040

Figure 4(a) shows the Dark Count Rate (DCR) versus the excess voltage. It grows linearly for all the design variants and is very similar in value for all of them. The DCR is below 80 kcps/mm^2 at 10 V of excess bias and below 250 kcps/mm^2 at 25 V of excess bias. This result shows that the new trench structure does not introduce additional defects in the silicon that could harm this important noise parameter. Moreover, it shows that the detector can be operated in a wide voltage range allowing the optimization of the bias condition. Above 25 V a sharp increase in DCR for all cell sizes is observed, suggesting the presence of an edge breakdown, which was observed also in the IV measurements.

The single cell gain (shown in figure 4(b)) is in line with the FBK NUV-HD technology, ranging between 6 and 10 millions of carriers at 10 V of excess bias, depending on the cell size. The extended operating range allows to reach very high gain, between 14 and 23 millions of carriers at 25 V of excess bias for cell size between 40 and 50 µm respectively. Being able to operate the detector at very large gain allows to simplify the readout electronics and reduce its power consumption, which is beneficial in many application that have strong power constraints, i.e. on satellites or in the readout of very large areas, in particular in cryogenic condition. For values of gain above 25 V of excess bias, the plot shows no significant variation from linearity, suggesting proper quenching of the avalanche in this region.

The effectiveness of the metal layer inside the deep trench isolation is assessed through the measurement of a reduction in direct crosstalk (CT) between neighboring cells by a factor larger than 10 compared to the previous technology, with the NUV-HD-MT SiPMs having a CT around 3% at 10 V of excess bias while the NUV-HD one surpassed 40% at the highest measurable excess bias of 9 V. This strong suppression of the optical crosstalk is reflected also at high excess bias values where, despite the very high gain of the NUV-HD-MT, the CT is measured to be between 8% and 11% for the different cell sizes at 25 V of excess bias. While the presence of the metal-filling in the trenches greatly reduces the internal crosstalk, it does not help to reduce the contribution of external crosstalk, i.e. from secondary photons exiting the SiPM and being reflected back by the package or by a scintillator placed on top of the SiPM [5]. The contribution of the external crosstalk was measured on packaged samples of the NUV-HD-MT in which a 200 µm glass layer is placed on the surface of the SiPM. As visible in figure 4(c), despite the contribution of the external crosstalk, these detectors could still operate at higher excess bias than bare die NUV-HD ones, with a total CT of 17% 25% at 10 V of excess bias, depending on the cell size.

The presence of the metal layer inside the trenches, acting as a reflector for the photons emitted during the avalanche, could lead to the absorption of such photons inside the silicon substrate. The photogenerated charge carriers can then diffuse towards the depletion region, causing either afterpulsing (AP) events or delayed crosstalk (DeCT) events. Measurements of AP and DeCT probability resulted in values below the sensitivity of the analysis method and are estimated to be below 1% even at the highest bias, thus verifying the absence of this effect and proving the effectiveness of the metal layer in the suppression of the direct crosstalk.

From these results it is also possible to explain the behavior of the of the IV curves of the NUV-HD and the NUV-HD-MT at high voltages. For the NUV-HD SiPM, the current divergence is around 10 V of excess bias: in this condition the DCR is still low while the crosstalk is very high, leading to an exponential increase of the SiPM current. On the other hand, for the NUV-HD-MT SiPMs, the current divergence happens at around 25 V of excess bias and it is not caused by CT,

2023 JINST 18 P05040

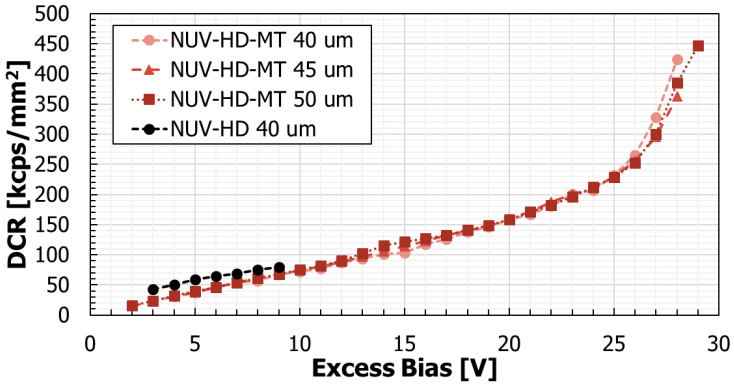

(a)

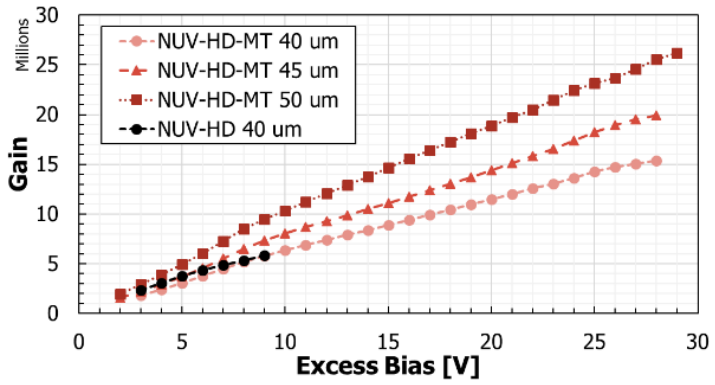

(b)

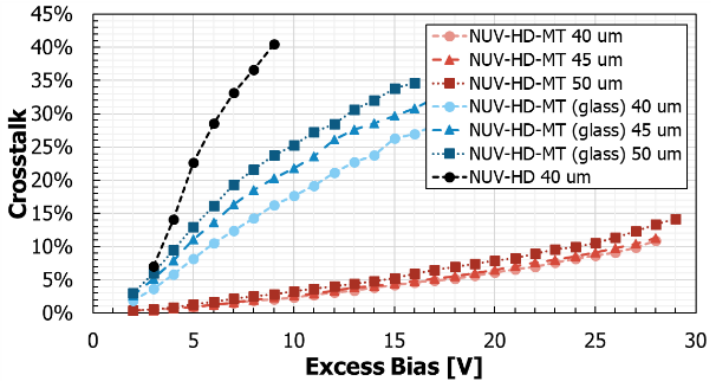

(c)

Figure 4. DCR (a), gain (b) and crosstalk probability (c) for three cell sizes of NUV-HD-MT packaged with bare die (shades of red) and with glass (shades of blue) and one cell size of NUV-HD packaged with bare die (black).

which is still relatively low, but rather by a fast increase of DCR caused by an edge breakdown of the SPAD.

Looking at the single microcell signal shape (figure 5) it is observed that, at the same excess bias of 8 V, and thus at the same gain for equal cell sizes, the recharge time constant (τ) of the signal is similar for the same cell size (40 µm) of the NUV-HD and the NUV-HD-MT. The metal filled version, though, shows a higher fast peak, compared to the standard version. This is likely related

2023 JINST 18 P05040

to the higher capacitive coupling of the metal grid layout to the SPAD junction that increases the parasitic capacitance (Cq) in parallel to the quenching resistor of the microcell [15]. Furthermore it can be seen that the amplitude of the fast peak increases with the cell size. Multiple factors contributes to this effect: larger area of Cq and a lower number of SPADs (for the same SiPM area) which reduces the filtering effect on the fast peak.

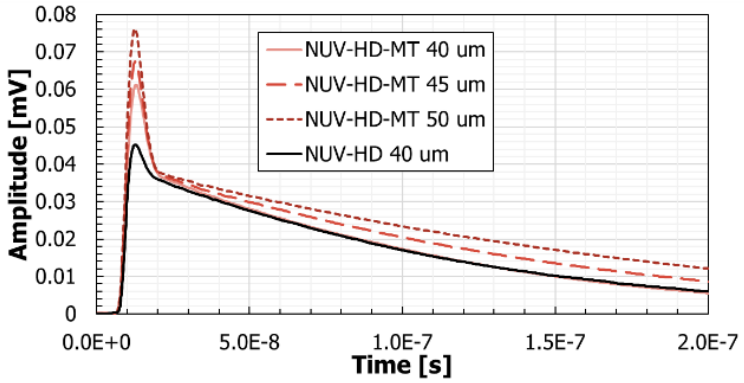

(a)

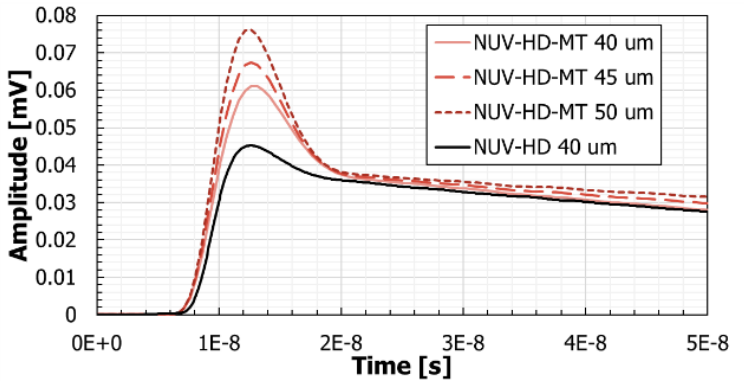

(b)

Figure 5. (a): most probable signal measured at 8 V of excess bias for three cell sizes of NUV-HD-MT (shades of red) and one cell size of NUV-HD (black). (b): detail of the fast peak for the same signals.

On the other hand, the larger diode capacitance reflects into a longer recharge time constant for the bigger cell, with the 50 µm cell having τ ~160 ns while smaller cells having τ ~120 ns (45 µm) and τ ~100 ns (40 µm), that is similar to the one of same cell size of the NUV-HD.

3.3 PDE

Photon detection efficiency was measured for the different cell sizes of NUV-HD-MT using the pulsed light method proposed in [16] that allows to remove the contribution of the correlated noise of the detector. The PDE was measured using different light emitting diodes (LEDs) with wavelengths ranging from 365 nm to 700 nm. The uncertainty on the measurement was estimated to be at 4% relative error. In order to better appreciate the difference in the PDE between the devices, the measured data were fitted using the formula:

$$\mathrm{PDE}\,(V_{\mathrm{Ex}}) = A \times \left(1 - \exp\left(\frac{-V_{\mathrm{Ex}}}{B + C \times \sqrt{V_{\mathrm{Ex}}}}\right)\right)$$

2023 JINST 18 P05040

Where V_{Ex} is the excess bias and A, B and C are the fit parameters. Figure 6(a) shows the measured and fit PDEs. It can be seen that PDE increases very quickly reaching 55 60%, depending on the SPAD size, at 5 V of excess bias and then it starts to saturate after 10 V of excess bias. Thanks to the large operating voltage range of the detector, however, it is possible to reach PDE in excess of 65%, depending on the cell size, at 20 V of excess bias. Comparing these results with the NUV-HD SiPM, there is no significant difference in PDE between the two technologies for the same cell size. On the other hand, the higher dynamic range of the NUV-HD-MT results in a 5% absolute PDE increase (8% relative increase) compared to the highest value obtained with the NUV-HD.

The PDE spectrum at different excess voltages as a result of the fit at each wavelength is show in figure 6(b). The spectrum of the PDE shows a peak in the near ultraviolet which is slightly shifting with the bias voltage. In particular at low bias, the peak is sharper and it is centered at 390 nm. On the other hand, at higher bias the peak is broader and almost flat between 390 nm and 420 nm. This change in shape of the PDE spectrum can be explained by the different contribution of the triggering probability of electrons and holes as a function of the excess bias. In particular, electrons have a higher triggering probability compared to holes at any excess bias and have a faster triggering probability increase with the excess bias. For this reason short wavelength photons, which are absorbed near the surface where electrons are the minority carriers, show a higher PDE with a faster increase with excess bias compared to longer wavelength, which are absorbed deeper in the junction, where holes are the minority carriers.

To better compare the two different technologies, it is useful to plot the performance parameters as a function of the PDE (figure 7). In figure 7(a), the DCR is plotted as a function of the PDE. It is interesting to notice that bigger cells have a smaller value of DCR at the same PDE compared to smaller cells, thanks to their higher FF. On the other hand the plot of gain vs. PDE (figure 7(b)) shows that the gain is the same for all the three SPAD sizes at the same PDE. Figure 7(c) shows the strong suppression of crosstalk in the metal-filled version: at 60% PDE the standard NUV-HD technology have around 35% probability, while in the new NUV-HD-MT technology this value is reduced by more than a factor of 10, with ~2% CT for all cell sizes at 60% PDE. When measuring the devices in a chip-sized package with cover glass, the contribution of the external CT the total value remains below the crosstalk value of the NUV-HD and does not exceed 15% at 60% PDE.

3.4 Timing

Besides the PDE, timing performance is an important figure of merit when it comes to the application in a ToF-PET apparatus. Two measurements are presented here: the first one is the Single Photon Time Resolution (SPTR) which depends only on the SiPM and the readout properties. The second one is the Coincidence Time Resolution (CTR), which is more representative of the final application in ToF-PET, using two SiPMs coupled to scintillating crystals.

SPTR was measured using a femtosecond laser with emission at 520 nm and ~150 fs FWHM pulse width, attenuated to single photon level by the use of a neutral density filter. The SiPM signal was amplified with a transimpedance amplifier circuit (based on an AD8000 operational-amplifier) and digitized with an Agilent oscilloscope MSO9104A with 1 GHz bandwidth and 20 GS/s sampling rate as described in detail in [17]. Measurements were taken both on single SPADs having the same design as the ones included in the SiPMs and on 1×1 mm^2 devices. Results are shown in figure 8. As it can be seen, the SPTR tends to saturate above 16 V of excess bias reaching a minimum of

2023 JINST 18 P05040

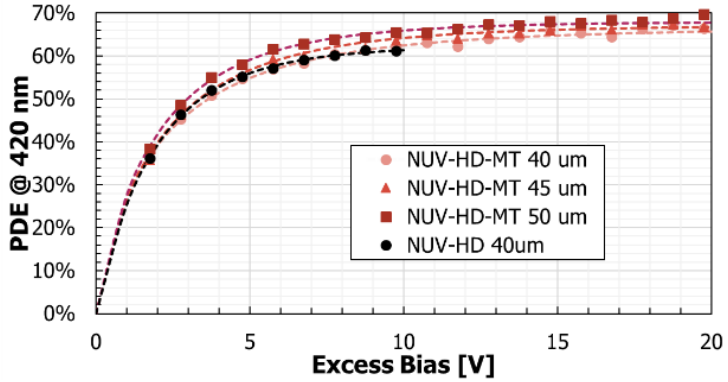

(a)

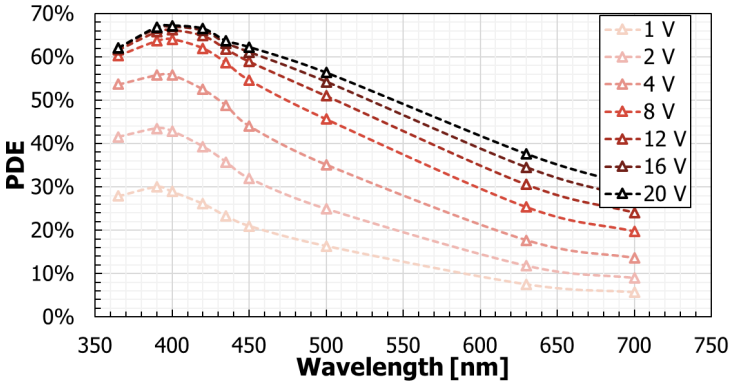

(b)

Figure 6. (a): PDE as a function of the excess bias measured at 420 nm for three cell sizes of NUV-HD-MT (shades of red) and one cell size of NUV-HD (black). The dots are the measured data while the dashed lines are the fit results. (b): PDE as a function of the wavelength measured at different excess bias voltages for the NUV-HD-MT SiPM with 45 µm cell size. The hollow triangles represent the PDE at the measured wavelengths, calculated from the fit of PDE vs. excess bias while the dashed lines are used as an eye guide.

55 ps FWHM for the $1 \times 1\,\mathrm{mm}^2$ SiPM with 45 µm cell size and 45 ps FWHM for the single SPAD with the same cell size. The smaller cell yielded slightly worse results for both detector sizes.

CTR measurements were performed using two $4 \times 4\,\mathrm{mm}^2$ SiPMs with the same cell size each coupled to a $3 \times 3 \times 5\,\mathrm{mm}^3$ LYSO:Ce,Ca crystal. The crystals were wrapped in ~10 PTFE layers (100 µm thickness each) in order to improve the light collection efficiency and they were coupled to the SiPMs using Cargille Meltmount optical glue ($n = 1.539$) [18]. The signal was readout through the same transimpedance amplifier circuit described above. In this case, one low-gain output measures the energy of the scintillation signal and discriminates the 511 keV gamma photons from Compton-scattered events, while the second output employs a pole-zero compensation to extract the timing information. The total of four output signal were measured with a 4-channel Agilent oscilloscope DSO9104A with 1 GHz bandwidth and 10 GS/s sampling rate per channel. The two detectors were facing each other with a ^{22}Na-source emitting pairs of 511 keV photons placed between them.

Results of CTR measurements are shown in figure 9. It can be seen that the CTR reaches similar minimum values of around 90 ps FWHM independently on the SPAD pitch. However, this

2023 JINST 18 P05040

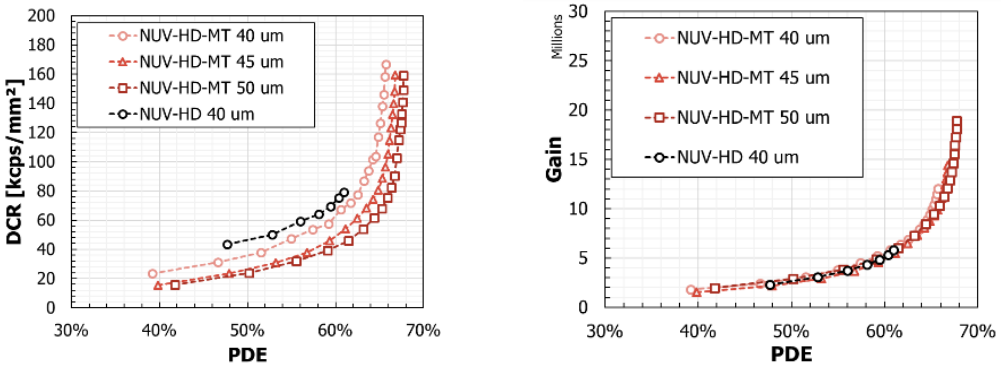

(a) (b)

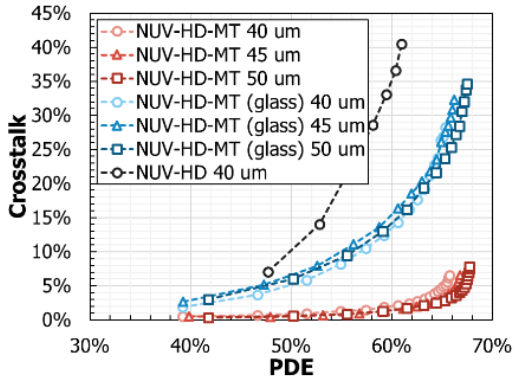

(c)

Figure 7. (a) to (c): DCR, gain and crosstalk probability as a function of the PDE measured for three cell sizes of NUV-HD-MT packaged with bare die (shades of red) and with glass (shades of blue) and one cell size of NUV-HD packaged with bare die (black). The hollow circles represent the data points with the PDE calculated from the fit of PDE vs. excess bias while the dashed line is used as an eye guide.

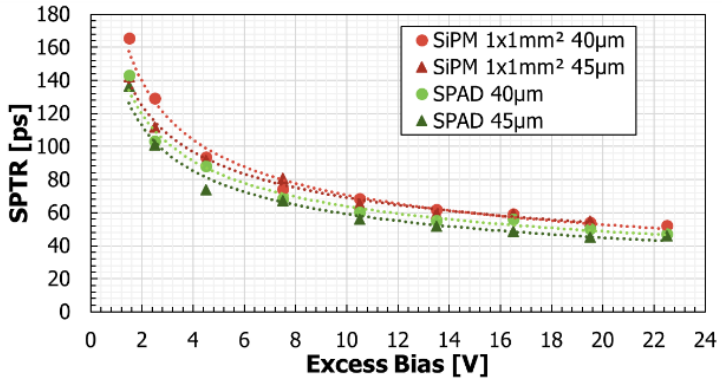

Figure 8. SPTR measured on $1 \times 1\,\mathrm{mm}^2$ SiPMs (shades of red) and for single SPADs (shades of green) for two different cell sizes of 40 µm and 45 µm. Dotted lines are used as a guideline.

value is reached at different excess bias voltages for the different SPAD pitches. In particular the larger, 50 µm, cell has a lower CTR at low excess bias due to its higher FF and PDE but the higher CT (both internal and external [5]), caused by its higher gain, limits the applicable excess bias to

2023 JINST 18 P05040

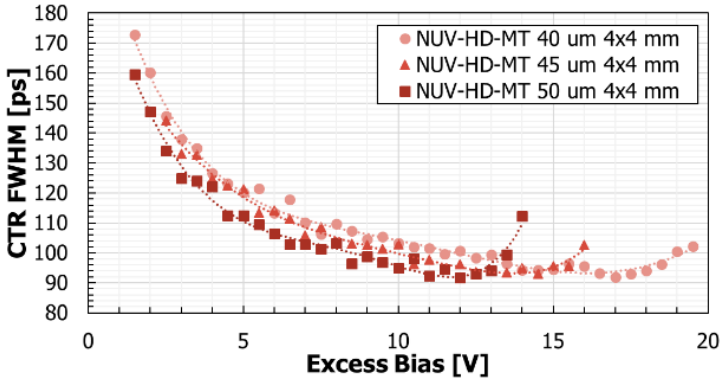

(a)

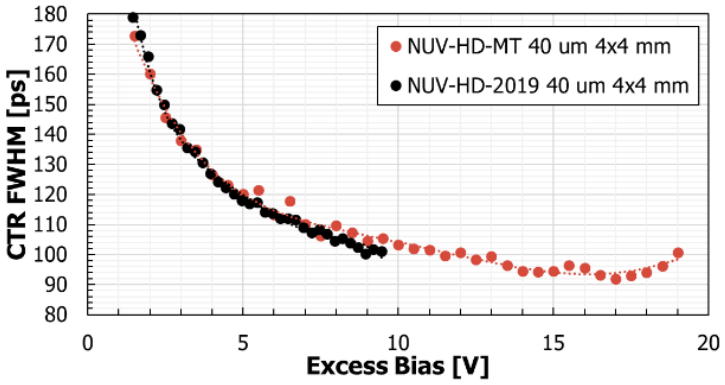

(b)

Figure 9. (a): CTR as a function of the excess bias for three cell sizes of the NUV-HD-MT. (b): comparison between NUV-HD-MT (red) and NUV-HD-2019 (black) with the same cell size.

about 12 V. On the other hand, smaller cells have a later CTR degradation due to the lower CT at a given excess bias. This allows to reach the same minimum value of CTR but at higher excess bias, i.e., 14 V and 17 V for the 45 µm and 40 µm cell respectively. Figure 9(b) compares these results with the ones reported in 2019 in ref. [8] on the NUV-HD technology (named for clarity NUV-HD-2019). It was not possible to directly compare the CTR of the NUV-HD-MT and the NUV-HD SiPMs used for the PDE measurements and the functional characterization in dark, as they have different sizes. Figure 9(b) shows that the suppression of the crosstalk in the NUV-HD-MT slightly shifts the minimum of the CTR towards higher excess bias and allows the detector to operate at higher PDE and gain values thus lowering the overall minimum of the CTR by about 5 ps. Although the improvement of the CTR is small, it is worth noticing that in the old technology the minimum was measured only for a narrow range of excess bias and very close to current divergence. This result can be obtained in a very well controlled laboratory condition but it might be difficult to achieve in a broader range of applications and in commercial medical imaging apparatus. In most applications the acceptable working condition for this sensor would be around 6–7 V of excess bias, thus limiting the CTR to ~110 ps. On the other hand, for the NUV-HD-MT, the CTR plot shows a much wider minimum which spans a range of about 5 V and can be beneficial in improving the performance of the full system in many applications where it is not feasible to have an extremely precise control of the bias voltage or of the temperature of the SiPM. In particular a recommended

2023 JINST 18 P05040

working condition for the NUV-HD-MT could be between 11 V and 16 V of excess bias, with CTR consistently below 100 ps.

3.5 Energy resolution

To highlight the different behaviour of the two technologies in terms of operating range and stability, we analyzed the energy spectrum and resolution of the 511 keV peak of ^{22}Na-source. For this measurement we acquired scintillation signals from a single detector of NUV-HD-2019 and NUV-HD-MT, both $4 \times 4\,\mathrm{mm}^2$ with 40 µm cell pitch. The acquired charge spectrum of the scintillation events was corrected by the system non-linearity [19] and converted into an energy spectrum by calibrating on the two main emission peak of ^{22}Na: 511 keV and 1274.5 keV. Figure 10(a) shows the measured energy spectrum for the two technologies, taken at 8.5 V of excess bias with an integration time of 500 ns. From this figure it is possible to see the two main peaks of the emission spectrum, with a small escape peak ~54 keV below the 511 keV peak and the Compton edge for lower energies. While the 511 keV peak is similar for the two technologies it can be seen that the 1274.5 keV peak is much broader for the NUV-HD technology. This is likely due to the higher crosstalk of this detector, which worsens the resolution for the high energy peak, when the detector is close to saturation. Figure 10(b) shows the energy resolution of the 511 keV peak for the two detectors, calculated at 500 ns of integration time. Both technologies show a similar behaviour at low excess bias, with energy resolution around 9.5% FWHM. Increasing the excess bias however, it can be seen that, while the energy resolution for NUV-HD-MT remains constant even at 12 V of excess bias, for the NUV-HD technology the energy resolution rapidly deteriorates above 7 V of excess bias. This confirms what stated above, that for the NUV-HD SiPM the best resolution is obtained very close to the current divergence and it is not at a stable point for operation. On the other hand NUV-HD-MT shows a much wider range of stability that allows to obtain better performances in commercial applications.

4 Conclusions

In the framework of a collaboration between FBK and Broadcom, we developed the NUV-HD-MT technology which improves the NUV-HD technology by introducing optically insulating deep trench isolation between SPADs. We have shown that the new technology features a strong suppression of the internal optical crosstalk by more than a factor of 10 compared to the previous one. This extends the operating range of the detector resulting in an increased PDE that exceeds 65% at 420 nm and in a SPTR of 55 ps for $1 \times 1\,\mathrm{mm}^2$ detectors and 45 ps for single SPADs with 45 µm cell size. While the external crosstalk is the same for NUV-HD and NUV-HD-MT when coupled to scintillating crystals, the overall reduction of the direct crosstalk enables to increase the operating dynamic range of the detector and results in an improved CTR with a minimum measured value of 90 ps FWHM with a wide operating bias range in the best timing region, which is expected to help with the stability of the detector when integrated in medical imaging apparatus.

Further advancement of this technology can be achieved by reducing the optical crosstalk when coupled to scintillating crystals. Especially for the larger cell sizes, this should allow to better operate the device and improve the CTR.

2023 JINST 18 P05040

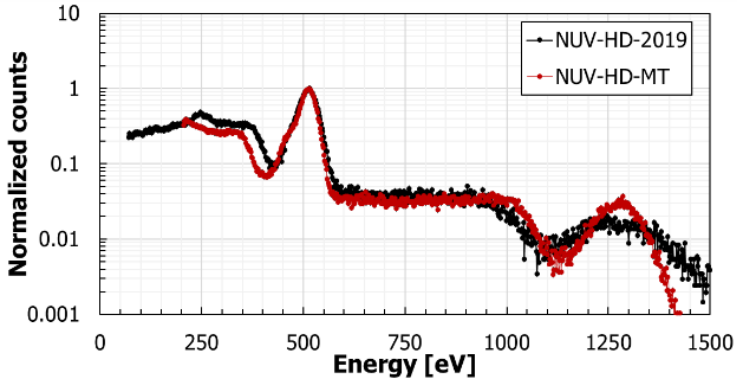

(a)

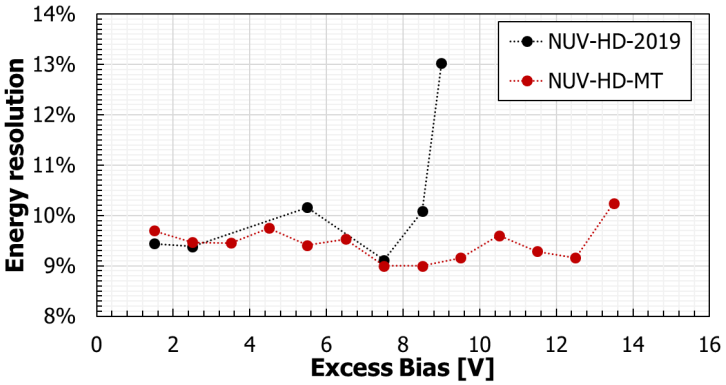

(b)

Figure 10. (a): energy spectrum for a ^{22}Na-source measured with a 4×4 mm^2 SiPM with 40 µm cell size for the NUV-HD-MT technology (red) and NUV-HD-2019 technology (black). (b): energy resolution for the 511 keV peak as a function of the excess bias for the two technologies, calculated at 500 ns of integration time.

Acknowledgments

Authors S. Brunner, A. Inglese and C. Piemonte declare that they are employed by Broadcom Inc. Broadcom Inc. commercializes products based on the NUV-MT technology.

Joint development of the NUV-HD-MT technology was funded by Broadcom Inc.

References

[1] P. Lecoq and S. Gundacker, *SiPM applications in positron emission tomography: toward ultimate PET time-of-flight resolution*, *Eur. Phys. J. Plus.* **136** (2021) 292.

[2] S. Gnecchi and C. Jackson, *A* 1×16 *SiPM array for automotive* 3*D imaging LiDAR systems*, in proceedings of the *2017 International Image Sensor Workshop (IISW)*, Hiroshima, Japan, 30 May–2 June 2017.

[3] C.E. Aalseth et al., *DarkSide-20k: A* 20 *tonne two-phase LAr TPC for direct dark matter detection at LNGS*, *Eur. Phys. J. Plus* **133** (2018) 131 [arXiv:1707.08145].

[4] K. Wagatsuma et al., *Comparison between new-generation SiPM-based and conventional PMT-based TOF-PET/CT*, *Phys. Med.* **42** (2017) 203.

2023 JINST 18 P05040

[5] A. Gola et al., *SiPM optical crosstalk amplification due to scintillator crystal: effects on timing performance*, *Phys. Med. Biol.* **59** (2014) 3615.

[6] S. Gundacker et al., *On the comparison of analog and digital SiPM readout in terms of expected timing performance*, *Nucl. Instrum. Meth. A* **787** (2015) 6.

[7] F. Acerbi et al., *Analysis of single-photon time resolution of FBK silicon photomultipliers*, *Nucl. Instrum. Meth. A* **787** (2015) 34.

[8] V. Oleynikov and V. Porosev, *After-pulsing and cross-talk comparison for PM1125NS-SB0 (KETEK), S10362-11-100C (HAMAMATSU) and S13360-3050CS (HAMAMATSU)*, 2017 *JINST* **12** C06046.

[9] A. Gola et al., *NUV-Sensitive Silicon Photomultiplier Technologies Developed at Fondazione Bruno Kessler*, *Sensors* **19** (2019) 308.

[10] F. Acerbi et al., *NUV Silicon Photomultipliers With High Detection Efficiency and Reduced Delayed Correlated-Noise*, *IEEE Trans. Nucl. Sci.* **62** (2015) 1318.

[11] R.J. McIntyre, *Theory of Microplasma Instability in Silicon*, *J. Appl. Phys.* **32** (1961) 983.

[12] R.H. Haitz, *Model for the Electrical Behavior of a Microplasma*, *J. Appl. Phys.* **35** (1964) 1370.

[13] S. Cova et al., *Avalanche photodiodes and quenching circuits for single-photon detection*, *Appl. d Opt.* **35** (1996) 1956.

[14] C. Piemonte et al., *Development of an automatic procedure for the characterization of silicon photomultipliers*, in proceedings of the *2012 IEEE Nuclear Science Symposium and Medical Imaging Conference Record (NSS/MIC)*, Anaheim, CA, U.S.A., 27 October–3 November 2012, IEEE (2012), pp. 428–432 [DOI:10.1109/nssmic.2012.6551141].

[15] F. Corsi et al., *Modelling a silicon photomultiplier (SiPM) as a signal source for optimum front-end design*, *Nucl. Instrum. Meth. A* **572** (2007) 416.

[16] G. Zappalà et al., *Study of the photo-detection efficiency of FBK High-Density silicon photomultipliers*, 2016 *JINST* **11** P11010.

[17] F. Acerbi et al., *Characterization of Single-Photon Time Resolution: From Single SPAD to Silicon Photomultiplier*, *IEEE Trans. Nucl. Sci.* **61** (2014) 2678.

[18] http://www.cargille.com/mounting-media/.

[19] V. Regazzoni et al., *Characterization of high density SiPM non-linearity and energy resolution for prompt gamma imaging applications*, 2017 *JINST* **12** P07001.

2023 JINST 18 P05040